Mercury Cratering Record Viewed from MESSENGER's First Flyby

Robert G. Strom, *et al.*

Science **321**, 79 (2008);
DOI: 10.1126/science.1159317

14. R. J. Pike, in *Mercury*, F. Vilas, C. R. Chapman, M. S. Matthews, Eds. (Univ. of Arizona Press, Tucson, AZ, 1988), pp. 165–274.
15. J.-L. Margot, D. B. Campbell, R. F. Jurgens, M. A. Slade, *J. Geophys. Res.* **104**, 11875 (1999).
16. R. J. Pike, *Proc. Lunar Planet. Sci. Conf.* **11**, 2159 (1980).
17. Surface roughness and small-scale tilts, and off-nadir ranging, which occurred at angles of up to 70° during the flyby, combine to spread MLA's reflected pulse. To maximize the probability of detecting spread returns, the returned pulse is passed through three matched filters after the detector amplifier, and subsequently time-to-digital converters are employed to measure the leading- and trailing-edge times of the pulse. MLA measures pulse widths between 6 and 1000 ns, corresponding to an RMS variation in range to the surface within each laser spot of 0.4 to 64 m (*2*, *19*).
18. These apparent slopes are likely minimum values.
19. J. B. Abshire, X. Sun, R. S. Afzal, *Appl. Opt.* **39**, 2449 (2000).

20. The MESSENGER project is supported by the NASA Discovery Program under contracts NAS5-97271 to Johns Hopkins University Applied Physics Laboratory and NASW-00002 to the Carnegie Institution of Washington. We acknowledge important contributions from the MLA instrument and MESSENGER spacecraft teams.

14 April 2008; accepted 3 June 2008
10.1126/science.1159086

REPORT

Mercury Cratering Record Viewed from MESSENGER's First Flyby

Robert G. Strom,[1]* Clark R. Chapman,[2] William J. Merline,[2] Sean C. Solomon,[3] James W. Head III[4]

Morphologies and size-frequency distributions of impact craters on Mercury imaged during MESSENGER's first flyby elucidate the planet's geological history. Plains interior to the Caloris basin displaying color and albedo contrasts have comparable crater densities and therefore similar ages. Smooth plains exterior to Caloris exhibit a crater density ~40% less than on interior plains and are thus volcanic and not Caloris impact ejecta. The size distribution of smooth-plains craters matches that of lunar craters postdating the Late Heavy Bombardment, implying that the plains formed no earlier than 3.8 billion years ago (Ga). At diameters less than or equal to 8 to 10 kilometers, secondary impact craters on Mercury are more abundant than primaries; this transition diameter is much larger than that on the Moon or Mars. A low density of craters on the peak-ring basin Raditladi implies that it may be younger than 1 Ga.

Mercury has been struck by asteroids and comets since it formed, resulting not only in primary impact craters of all sizes but also in secondary craters made by reimpact of ejecta from the primary craters. Such secondaries typically have morphologies different from the pristine shapes of primary craters, and many secondary craters form clusters and chains. Geological processes such as faulting, volcanism, downslope motion, and continued cratering all degrade crater shapes, eventually erasing them by erosion or covering. The statistics of crater sizes, shapes, and spatial relations—especially their size-frequency distributions (SFDs) (*1*)—provide information (including relative ages) about the processes that formed and reshaped the cratered landscapes.

Images of Mercury by Mariner 10 from 1974 to 1975 and subsequent studies of other planetary surfaces have raised issues that the MESSENGER mission to Mercury can address (*2*), including the relative importance of secondary versus primary cratering and of volcanic versus impact-ejecta modes of plains formation. During its first flyby of Mercury, the MESSENGER spacecraft imaged portions of a crater-scarred landscape never before seen at close range. These images show the entire 1550-km-diameter Caloris impact basin (*3*) and a broad surrounding annulus of smooth plains. They also reveal diverse cratered terrains, some nearly saturated with large craters but others very sparsely cratered. Here we report preliminary analyses of crater morphology and SFD measurements from several selected regions, based chiefly on images from the narrow-angle camera (NAC) of the Mercury Dual Imaging System (*4*).

Observations of the Moon and Mars have shown that craters in the inner solar system have two SFD components (*5*, *6*). Terrains with a high density of large craters have a complex differential SFD that approximately follows a power law with a slope of –2 for crater diameter D = ~2 to 50 km. This "Population 1" was formed primarily during the Late Heavy Bombardment (LHB), characterized by large impact basins such as the Caloris basin on Mercury, only part of which was seen by Mariner 10. Younger surfaces have an SFD with a slope of –3 ("Population 2"). (Figure S1 summarizes these two SFDs.) Both impactor populations were probably derived originally from the asteroid belt (*6*). Population 1 may have resulted from size-independent ejection as gravitational resonances swept through the belt during giant-planet migration ~4 billion years ago (Ga) (*7*, *8*). Population 2 reflects impacts of near-Earth asteroids (NEAs), mainly derived by the size-dependent Yarkovsky effect that causes smaller main-belt asteroids to preferentially enter resonances and be placed into planet-crossing orbits (*9*, *10*). Heavily cratered regions of Mercury have a SFD similar to that of the highlands of the Moon and Mars (Fig. 1A). However, on Mercury and Mars, there is a dearth of craters with D < 40 km relative to the Moon (*11*). On Mercury, smaller craters were apparently removed by the formation of "intercrater plains" (*12*) during the LHB (different processes erased smaller Martian craters). The shapes of the SFDs for Mercury, Mars, and the Moon for D = 40 to 150 km (a range not affected by intercrater plains and with good statistics) match each other better if shifted somewhat in diameter, apparently because heliocentrically orbiting NEAs collide with Mercury at higher velocities and Mars at lower velocities as compared with the Moon (fig. S4).

MESSENGER data show that the northwestern half of the Caloris floor has a slightly lower albedo and different color than the southeastern half (Fig. 1C) (*3*). Could these two plains regions have been formed by volcanic episodes at widely different times? SFDs (for D > 10 km, craters unlikely to be secondaries) for these regions (Fig. 1B) (as well as for an east/west division) show no significant differences, so their ages are comparable within 10 to 20%. Until we can measure crater densities on the Caloris rims and ejecta, we cannot determine if the flooding of the floor was contemporaneous with the impact (e.g., by impact melt) or occurred later; the uncertainties nonetheless permit a lengthy period for emplacement of successive volcanic flows, particularly if they occurred after the end of the LHB when the cratering rate was low.

Since the Apollo-era discovery that the Cayley plains on the Moon were basin impact ejecta rather than of volcanic origin, a major issue in planetary geology has concerned the relative importance of volcanism in plains formation. The crater density on some of the darker exterior smooth plains that form an annulus around Caloris is about 40% lower than that on plains inside Caloris (Fig. 2A), which is consistent with

[1]Lunar and Planetary Laboratory, University of Arizona, Tucson, AZ 85721, USA. [2]Southwest Research Institute, 1050 Walnut Street, Suite 300, Boulder, CO 80302, USA. [3]Department of Terrestrial Magnetism, Carnegie Institution of Washington, 5241 Broad Branch Road, NW, Washington, DC 20015, USA. [4]Department of Geological Sciences, Brown University, Providence, RI 02912, USA.

*To whom correspondence should be addressed. E-mail: rstrom@lpl.arizona.edu

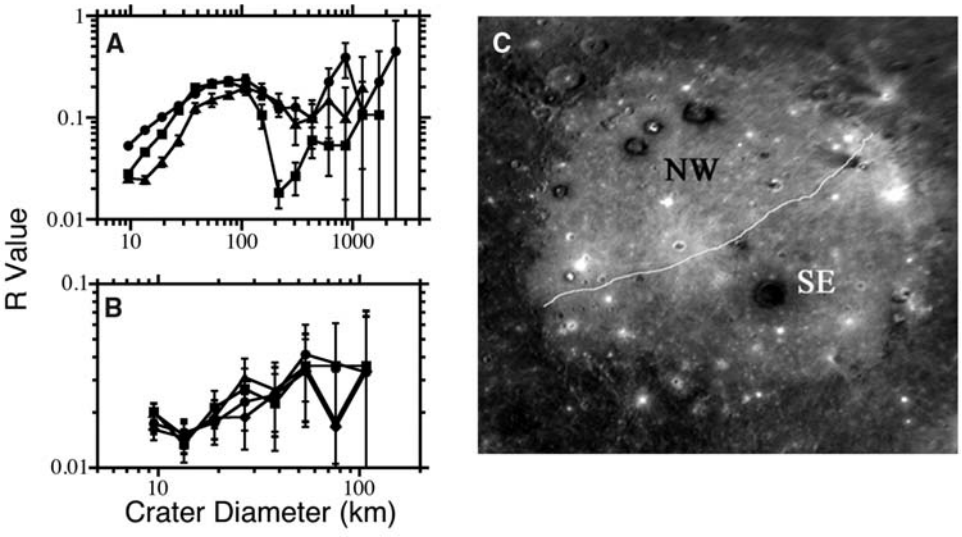

Fig. 1. (**A**) Crater SFDs for heavily cratered surfaces on the Moon (circles), Mars (squares), and Mercury (triangles) [from (*11*)]. Mars and Mercury have a deficit of craters at $D < 40$ km. The upturn at 10 km for Mercury could be the start of the secondary branch (Fig. 4). The format of this diagram (and of others in this paper) is the log-log R plot, a version of the differential SFD (*1*, *24*). Error bars in all figures indicate $\sqrt{(N)}/N$ SDs and do not account for uncertain systematic errors. (**B**) Crater SFDs of the northwestern (triangles) and southeastern (diamonds) portions of the Caloris interior plains, and separately of the eastern (circles) and western (squares) halves of the basin. Crater densities for all four sectors are the same to within 10 to 20%. (**C**) MESSENGER image of the Caloris basin showing the regions of the interior plains having slightly different colors and albedos (*3*) for which craters were counted.

a Mariner 10 study in a smaller area (*13*). Thus, the exterior smooth plains were emplaced after the interior plains and must be volcanic units rather than ejecta deposits from the Caloris impact. The SFDs for the exterior and interior plains have shallower slopes than the SFDs for heavily cratered terrains, so the craters must be largely Population 2. Although the smooth plains contain some slightly degraded craters, most are fresh with well-defined ejecta deposits and have a Population 2 SFD like fresh lunar craters (Fig. 2B). Hence, the exterior plains formed near or after the end of the LHB at ~3.8 Ga and well after Caloris (*14*).

The issue of whether secondaries are a minor or dominant contributor to small crater populations on planets and satellites has been controversial since the 1960s. On the basis of the steeply sloped SFD of lunar craters <2 km in diameter (resembling the D^{-5} SFD for secondaries of the lunar crater Langrenus), Shoemaker originally hypothesized that most small lunar craters are secondaries (*15*, *16*). More recently, it has been proposed (*17*) that this steep branch of the SFD is an inherent part of the primary crater SFD due to NEAs, but small secondaries have been shown to predominate on bodies as diverse as Europa and Mars (*18*–*20*). The degree to which secondary craters dominate crater populations remains controversial.

Clusters of secondaries, seen in some higher-resolution Mariner 10 images (*21*), were presumed to constitute a minor fraction of Mercury's smaller craters. MESSENGER images suggest that secondary cratering is much more important than had been thought, as exemplified by the many distinct chains and clusters of craters radiating away from prominent, large, fresh impact craters and basins. We characterized the secondary crater SFD for Mercury from craters within the overlapping secondary crater fields

Fig. 2. Comparison of SFDs for the Caloris interior and exterior plains (Fig. 1B) as well as lunar highlands and fresh craters. (**A**) Circles represent the lunar highlands. The Caloris interior plains (squares) show a ~40% greater crater density than that of the exterior plains (triangles). (**B**) SFD for Caloris exterior plains (squares) slopes gently down to the left but is similar to the SFD for fresh lunar frontside craters (circles), indicating that the exterior (and interior) plains consist mainly of Population 2 craters.

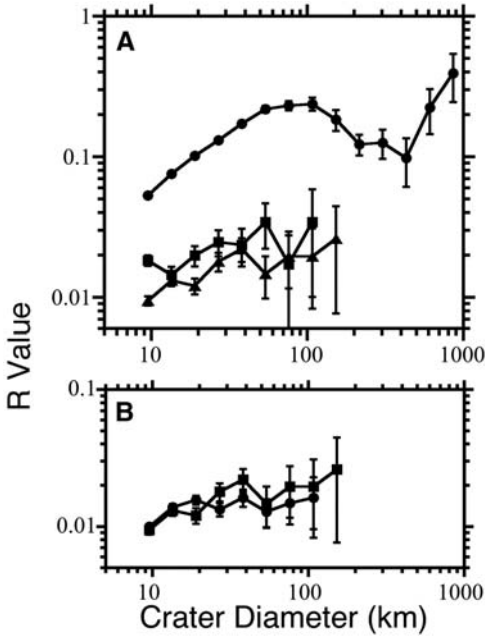

of three large, fresh primary craters and one smaller, rayed crater. The SFD slope (open diamonds in Fig. 3) for $4 < D < 10$ km is steep (at least –5) like that for lunar secondaries. More than half of these craters are in obvious clusters or chains, and >90% of craters with $2 < D < 4$ km are clustered; a major fraction of these must be secondaries because primary craters are spatially random. Also, ~90% of craters with $D < 10$ km have nonpristine shapes, characteristic of secondary craters. The actual proportion of secondaries in this region could be still higher, because high-velocity ejecta from more distant primaries make secondaries that are less obviously clustered and are more nearly bowl-shaped. SFDs for the other localities plotted in Fig. 3 (all generally far from obvious secondary crater fields) are also steep for $D <$ 8 km (although steeper for the heavily cratered study area than for the plains west of Caloris), suggesting that secondaries dominate the small crater populations to varying degrees in these diverse terrains on Mercury.

Craters making up the steep secondary branch of SFDs begin to dominate over the primary SFD at a much larger diameter on Mercury than on the Moon, Mars, or other bodies (Fig. 4). The reason is not clear, but it was recognized from some Mariner 10 images (*22*) that secondaries on Mercury seem to be better preserved than those on the Moon. The density of impact basins on Mercury is about the same as on the Moon (Fig.

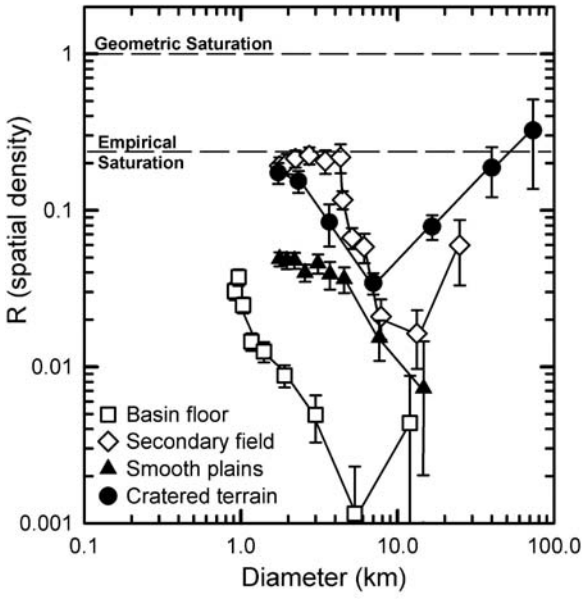

Fig. 3. SFDs for various surfaces on four frames from a NAC mosaic (frame locations are shown in fig. S3). The upturn at $D < \sim 8$ km is due to secondaries. For $2 < D < 4$ km in the secondary crater field, the SFD cannot continue upward to still higher density; consequently it must bend over to follow a −3 slope at the empirical saturation density. Note the very low density of craters on the floor of the peak-ring basin Raditladi (see text).

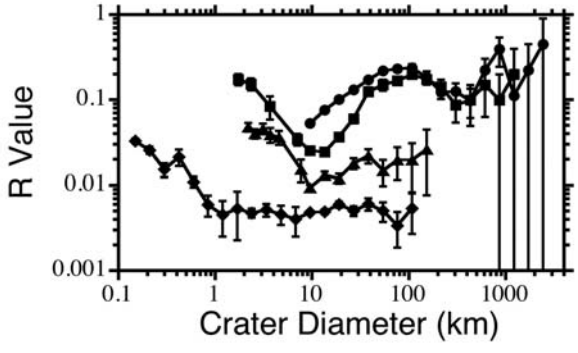

Fig. 4. Comparison of the lunar highlands (circles), heavily cratered terrain on Mercury (squares), Caloris exterior smooth plains (triangles), and young Martian surfaces (diamonds). The Mars SFD is a composite of young plains for $D > 0.2$ km. The upturn at $D < 1$ km is primarily attributable to secondaries (*20*). On Mercury, the upturn occurs at $D <$ 10 km and is due to secondaries. (On all terrestrial bodies, there may be a minority of craters >10 km that are secondaries from large basins.)

1A), so one might expect a comparable number of secondaries. Perhaps basins such as Caloris and the newly imaged peak-ring basin Raditladi are unusually youthful so that their secondaries are better preserved. Surface gravity cannot be responsible because it is similar on Mercury and Mars. Fragment size should be inversely proportional to impact velocity (*23*); thus, secondaries should be smaller on Mercury, where impact velocities are higher than those on the Moon and Mars. The larger secondaries may be the result of differences in material strength of the target material so that larger fragments are produced. In any event, the use of small craters for dating of geological units on Mercury must be done with even greater caution than is needed for other bodies. Whereas an older unit will tend to have more secondaries on it than a younger unit, there cannot be the one-to-one correspondence of crater density with relative or absolute age (as there is for primary craters) because of the temporally and spatially nonuniform production of secondaries.

The density of small craters on the floor of Raditladi is an order of magnitude lower than that of the plains west of Caloris, whereas the density on small craters on Raditladi's ejecta deposits is similar to that of its floor (Fig. 3). These results do not require that Raditladi is $^1/_{10}$ of the age of the plains, because it may have been formed when the cratering rate was changing rapidly as the LHB ended, compressing the time scale. Spatial densities of secondary craters vary, even across surfaces of the same age, but Raditladi is located near the apparently much older smooth plains that we sampled, so it is possible that Raditladi and its interior plains were formed within the last billion years. If the plains within Raditladi were formed by volcanic processes rather than being impact melt, then Mercury's geological activity may have persisted (at least locally) into comparatively recent epochs rather than ending shortly after the LHB.

References and Notes

1. In this paper, we display the crater SFDs using the "Relative" plot. For an R plot, the differential SFD is divided by $dN(D) \sim D^{-3}dD$ (where N is the number of craters within a diameter increment), because most crater SFDs are well described by a power law having an exponent within ±1 of −3. A −3 distribution plots as a horizontal line, a −2 distribution slopes down to the left at an angle of 45°, and a −4 distribution slopes down to the right at 45°. The vertical position measures crater density: The higher the position, the higher the crater density and the older the surface. Although ideally craters could be packed together so that spatial density $R = 1$, in reality cratered surfaces rarely exceed the empirical saturation density with $R \sim 0.2$ to 0.25.
2. J. W. Head *et al.*, *Space Sci. Rev.* **131**, 41 (2007).
3. S. L. Murchie *et al.*, *Science* **321**, 73 (2008).
4. S. E. Hawkins III *et al.*, *Space Sci. Rev.* **131**, 247 (2007).
5. R. G. Strom, S. K. Croft, N. G. Barlow, in *Mars*, H. H. Kieffer, B. M. Jakosky, C. Snyder, M. S. Matthews, Eds. (Univ. of Arizona Press, Tucson, AZ, 1992), pp. 383–423.
6. R. G. Strom, R. Malhotra, T. Ito, F. Yoshida, D. A. Kring, *Science* **309**, 1847 (2005).
7. K. Tsiganis, R. Gomes, A. Morbidelli, H. G. Levison, *Nature* **435**, 459 (2005).
8. R. Gomes, H. F. Levison, K. Tsiganis, A. Morbidelli, *Nature* **435**, 466 (2005).
9. A. Morbidelli, D. Vokrouhlicky, *Icarus* **163**, 120 (2003).
10. W. F. Bottke, D. Vokrouhlicky, D. P. Rubincam, D. Nesvorny, *Annu. Rev. Earth Planet. Sci.* **34**, 157 (2006).
11. R. G. Strom, G. Neukum, in *Mercury*, F. Vilas, C. R. Chapman, M. S. Matthews, Eds. (Univ. of Arizona Press, Tucson, AZ, 1988), pp. 336–373.
12. "Intercrater plains" are a type of terrain recognized on Mercury, the Moon, and other planets characterized by nearly level plains sprinkled with small craters interspersed among a moderate density of large craters. Their mode of formation has been controversial.
13. P. D. Spudis, J. E. Guest, in *Mercury*, F. Vilas, C. R. Chapman, M. S. Matthews, Eds. (Univ. of Arizona Press, Tucson, AZ, 1988), pp. 118–164.
14. From Mariner 10 images, Neukum (*11*) estimated the age of the Caloris exterior plains at 3.85 Ga (near the end of the LHB), on the basis of a calibration with the lunar cratering record.
15. E. M. Shoemaker, in *Physics and Astronomy of the Moon*, Z. Kopal, Ed. (Academic Press, New York, 1962), pp. 283–359.
16. E. M. Shoemaker, in *The Nature of the Lunar Surface*, W. N. Hess, D. H. Menzel, J. A. O'Keefe, Eds. (Johns Hopkins Univ. Press, Baltimore, 1965), pp. 23–77.
17. G. Neukum, B. A. Ivanov, W. K. Hartmann, in *Chronology and Evolution of Mars* (Kluwer Academic, Dordrecht, Netherlands, 2001), pp 55–86.
18. E. B. Bierhaus, C. R. Chapman, W. J. Merline, *Nature* **437**, 1125 (2005).
19. A. S. McEwen, B. S. Preblich, E. P. Turtle, *Icarus* **176**, 351 (2005).
20. A. S. McEwen, E. B. Bierhaus, *Annu. Rev. Earth Planet. Sci.* **34**, 535 (2006).
21. D. E. Gault, J. E. Guest, J. B. Murray, D. Dzurisin, M. C. Malin, *J. Geophys. Res.* **80**, 2444 (1975).
22. D. H. Scott, *Phys. Earth Planet. Inter.* **15**, 173 (1977).
23. H. J. Melosh, *Geology* **13**, 144 (1985).
24. Crater Analysis Techniques Working Group, *Icarus* **37**, 467 (1979).
25. We thank M. Banks, who did many of the crater counts and helped with the analyses. The MESSENGER project is supported by the NASA Discovery Program under contracts NAS5-97271 (to the Johns Hopkins University Applied Physics Laboratory) and NASW-00002 (to the Carnegie Institution of Washington).

Supporting Online Material

www.sciencemag.org/cgi/content/full/321/5885/79/DC1
SOM Text
Figs. S1 to S4

18 April 2008; accepted 4 June 2008
10.1126/science.1159317